Prototype for Wireless Power Supply In-Wheel PMSM Considering Load Conditions

Ali Jafer Mahdi
College of Information Technology Engineering, Al-Zahraa University for Women, Karbala, Iraq | Department of Electrical and Electronics Engineering, University of Kerbala, Karbala, Iraq
ali.j.mahdi@alzahraa.edu.iq (corresponding author)

Haider Hameed Hussein
Department of Governorate Police Command - Planning and Follow-up, Karbala, Iraq
hayder.hameed@s.uokerbala.edu.iq

Ali Mohammed Ridha
College of Medicine, University of Al-Ameed, Karbala, Iraq
alialmosawi@alameed.edu.iq

Mohammed Jamal Mohammed
College of Dentistry, University of Al-Ameed, Karbala, Iraq
eng.mohammed.j@alameed.edu.iq

Hussban Abood Saber
Department of Electrical and Electronic Engineering, University of Kerbala, Karbala, Iraq
hussban.a@s.uokerbala.edu.iq

Mustafa Habeeb Chyad
University of Warith Al-Anbiyaa, Karbala, Iraq
mustafa.ha@uowa.edu.iq

Received: 26 January 2025 | Revised: 23 February 2025 | Accepted: 27 February 2025

 DOI: https://doi.org/10.48084/etasr.10350

ABSTRACT

This research presents the practical implementation of a Wireless Power Transfer (WPT) system for supplying an in-wheel Permanent Magnet Synchronous Motor (PMSM). The proposed system is designed to transfer approximately 250 W using a resonant circuit, with power delivery and motor performance regulated through DC-DC converters. The system is tested under various load conditions, including quarter-load, half-load, and full-load, ensuring stable operational speed and efficient performance in all cases. Key control parameters, including the duty cycle of the DC-DC converters and the system's resonant frequency, were examined for their impact on performance. Fine-tuning these parameters enabled efficient power transfer, reduced energy losses, and ensured system stability during dynamic transitions, particularly from half to full load. Furthermore, the voltage and current waveforms are presented and conformed to meet standard specifications, ensuring the system operates reliably and within acceptable limits. Practical experiments demonstrated the system's ability to achieve a measured efficiency of 94% at an air-gap distance of 7.5 cm under full load conditions. This highlights the system's potential for real-world applications, such as In-Wheel Motors (IWM) for Electric Vehicles (EVs), where reliability, efficiency, and stability are critical for overcoming challenges like power interruptions caused by vibrations.

Keywords-wireless power transfer; Inductive Wireless Power Transmission (IWPT); electric vehicles; DC-DC power converters

I. INTRODUCTION

Electric Vehicles (EVs) represent a promising solution for significantly reducing the environmental impact of road transport, particularly in terms of air pollution, carbon dioxide emissions, and noise [1]. Wireless Power Transfer (WPT) enables non-contact charging of EVs through electromagnetic coupling between transmitter and receiver coils [2]. The DC power stored in the battery is transferred via this spaced electromagnetic connection, while power transfer efficiency depends on the coupling coefficient, which is largely determined by the air gap between the coils [3, 4]. Coordinated control strategies are essential for maintaining system stability and enabling power-assisted steering in integrated electro-mechanical drive systems [5]. WPT systems operating in the radio frequency range (250 MHz to 1 THz) can transfer energy over long distances with high efficiency [6, 7]. In contrast, near-field WPT systems rely on electromagnetic coupling between coils to transfer energy via electric and magnetic fields. System efficiency and maximum power transfer are critical to optimizing WPT performance, particularly in relation to design characteristics [8].

WPT charging can be implemented using either stationary or dynamic methods. In the stationary configuration, the EV is parked over a wireless charging pad. In this case, the absence of physical conductors offers convenience, but a persistent challenge lies in maintaining efficient power transfer across the air gap between coils [9, 10]. The high air space built between wireless transfer coils damages the joint factor and destroys the efficiency transmitted. Moreover, conventional drivetrain configurations using a driveshaft may also lead to power losses, reduced range, and response delays between motor and wheel rotation. To address these issues, some EV manufacturers have adopted hub motors, or In-Wheel Motor (IWM) [11, 12]. In this design, the motor and drive electronics are integrated directly into each wheel, eliminating the need for a driveshaft. This setup minimizes power losses associated with mechanical components and allows individual control of each wheel, improving torque response and acceleration. Moreover, IWMs enhance space utilization and vehicle handling, enabling more precise cornering through independent left/right wheel control [13-15]. However, connecting wheel-mounted motors to the central battery pack via wiring poses practical challenges, like wires routed through the chassis to the wheels are susceptible to wear due to constant motion, steering, and environmental exposure. These durability issues can be effectively mitigated by employing WPT to deliver power wirelessly from the vehicle body to the wheel motors, eliminating the need for physical connections. These benefits have attracted increasing interest from both researchers and industry stakeholders in Wireless-IWM (W-IWM) [16]. The first generation, W-IWM1 [17], represents a practical application of WPT for eliminating wired power lines between the vehicle body and IWMs. The system supports bidirectional WPT, enables regenerative braking, and successfully transmits 3.3 kW to the wheels with an efficiency of 94.3%. The second generation, W-IWM2 [18, 19], further enhances performance by enabling WPT from the wheel-side coil back to the body-side coil, facilitating improved regenerative braking. This was achieved using a Lithium-ion Capacitor (LiC) located on the wheel side.

This paper contributes to the development and experimental validation of a W-IWM system using inductive coupling—a simpler, more robust, and practical alternative to magnetic resonance coupling. The system comprises two planar spiral coils: a stationary transmitter coil mounted on the vehicle body and a receiver coil integrated into the wheel. The transmitter operates within a frequency range of 50–250 kHz, providing the necessary conditions for efficient power transfer. A 250 W prototype was constructed and tested across various transmission distances, up to 12 cm, to evaluate real-world performance. In parallel, a simulation model was developed to validate and complement experimental findings, offering a theoretical foundation and computational confirmation of the system's performance.

II. MODELING AND ANALYSIS

The proposed system is demonstrated in Figure 1, consisting of two power converters on the transmitting (Tx) and receiving (Rx) sides. These are magnetically coupled through mutual inductance M(H). The voltage (V) equations governing the Tx and Rx loops are:

$$V_S = (R_T + j\omega L_T)I_T + j\omega M I_R \quad (1)$$

$$V_S = (R_R + R_L + j\omega L_R)I_R = -j\omega M I_T \quad (2)$$

where subscript T refers to the transmitter coil, the subscript R to the receiver coil, and subscript L to the load, R is the resistance (Ω), j is the imaginary unit, ω is the angular frequency (rad/s), L is the inductance (H), and I is the current (A)

By defining loop impedances as $Z_T = R_T + j\omega L_T$ and $Z_R = R_R + R_L + j\omega L_R$, the transmitter and receiver currents are expressed as:

$$I_R = -\frac{V_S j\omega M}{Z_R Z_T + M^2\omega^2} \quad (3)$$

With an input power, P_{in} and an output power, P_o, input complex power is expressed as follows [3]:

$$S_{in} = V_S^2 \frac{Z_R Z_T + M^2\omega^2}{|Z_R Z_T + M^2\omega^2|^2} Z_R^* \quad (4)$$

where Z_R^* is the complex conjugate of receiver impedance, and real input active power is expressed as:

$$P_{in} = Re\left(V_S^2 \frac{Z_R Z_T + M^2\omega^2}{|Z_R Z_T + M^2\omega^2|^2} Z_R^*\right) \quad (5)$$

and output power is expressed as:

$$P_o = |I_R|^2 R_L = \frac{{V_S}^2\omega^2 M^2}{|Z_R Z_T + M^2\omega^2|^2} R_L \quad (6)$$

Neglecting internal coil resistances, the simplified transmission efficiency is:

$$\eta = \frac{\omega^2 M^2}{R_L + \omega^2 M^2} \quad (7)$$

The quality factors Q_T and Q_R are:

$$Q_T = \frac{\omega L_T}{R_T},\ Q_R = \frac{\omega L_R}{R_R} \quad (8)$$

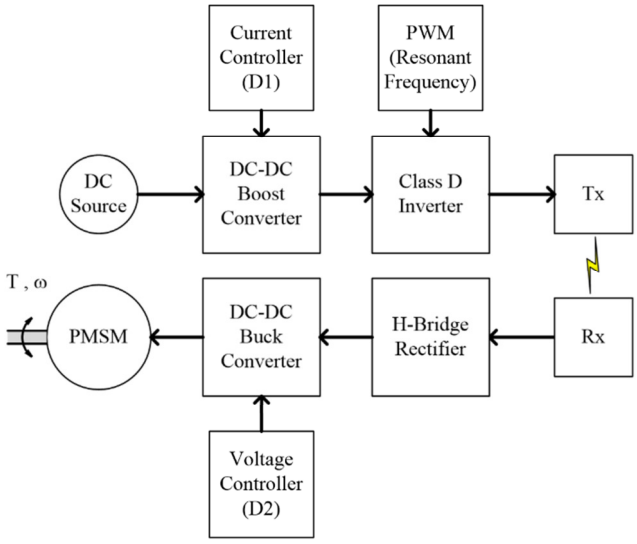

Fig. 1. The construction design of the planned system showing the three modules.

The current waveform can be mathematically described using Kirchhoff's Voltage Law (KVL) around the upper R_L loop as:

$$V_1 - i(t)R - L\frac{di(t)}{dt} = 0 \quad (9)$$

The equation directly above signifies the linear differential equation that can be solved as:

$$i(t) = \frac{V_1}{R} + Be^{\frac{-t}{\tau}} \quad (10)$$

$$i(t) = \frac{V_1}{R}\left(1 - e^{\frac{-t}{\tau}}\right) - I_L e^{\frac{-t}{\tau}} \quad (11)$$

Maximum rate of the inductance current, I_L, is attained at end of first half cycle. At this stage the time immediate $t = DT$ shall be substituted in (11) as follows:

$$I_L = \frac{V_1}{R}\left(\frac{1-e^{\frac{-DT}{\tau}}}{1+e^{\frac{-DT}{\tau}}}\right) \quad (12)$$

The coupling model consists of two identical coils. The inductive parameters of the coils are determined in terms of their design parameters. In inductive WPT systems, two coil topologies are used: spiral and helical. In the proposed system, the former geometry is used. One advantage of using spiral coils in loosely coupled systems is that their flux density is more uniform throughout the coil's surface, resulting in a higher coupling coefficient than helical coils [20]. This coil is designed and implemented using the online tools Coil64 [21], and [22] Flat Spiral Coil Calculator [22], which is another open-source online free-ware for calculating coil inductance. When using the online tool Coil64, calculates coil self-inductance by using the following formula,

$$L\,(\mu H) = r^2 \cdot \left(\frac{N^2}{(8r+11w)}\right) \quad (13)$$

where L represents the coil's self-inductance (μH), r is the average winding radius (in), w is the winding width (in), and N is the amount of turns in the coil. The transmitter's voltage, current, and phase coupling coefficient are reconfigured into a T-type equivalent circuit. In this model, the coil capacitances are represented as C_T and C_R, while the internal resistance of the transmitter voltage basis is included as Z_s. By examining the circuit from the contribution terminal, the input impedance Z_{in} can be expressed as:

$$Z_{in} = \frac{V_T}{I_T}(\cos\varphi + j\sin\varphi) \quad (14)$$

Therefore, the real and imaginary mechanisms of Z_{in} can be expressed as:

$$Re[Z_{in}] = R_T + \frac{(\omega M)^2(R_L+R_R)}{(R_L+R_R)^2+[\omega L_R-(1/\omega C_R)]^2} \quad (15)$$

$$Im[Z_{in}] = [\omega L_T - (1/\omega C_T)] - \frac{(\omega M)^2[\omega L_R-(1/\omega C_R)]}{(R_L+R_R)^2+[\omega L_R-(1/\omega C_R)]^2} \quad (16)$$

Examining the imaginary component in (17), it becomes clear that measuring this part is difficult because it is highly dependent on frequency. Consequently, the mutual induction will be estimated by measuring only real elements, as follows.

$$M = \frac{1}{\omega}\sqrt{\frac{[Re[Z_{in}]-R_T][(R_L+R_R)^2+[\omega L_R-[(1/\omega C_R)]^2]}{R_L+R_R}} \quad (17)$$

The coupling coefficient will be calculated using:

$$K = \frac{M}{\sqrt{L_T L_R}} \quad (18)$$

The coupling coefficient is influenced by the distance between joint coils; thus, it was evaluated at various separations to establish a typical relationship between the coupling factor K and the transmission distance d. Identical spiral coils were constructed, each with an outer diameter of 260 mm, an inner diameter of 50 mm, and 16 turns spaced 5 mm apart. A 9-meter length copper wire with a diameter of 2 mm was used for each coil. The wire was positioned in a circular groove carved into a square MDF base to provide structural support and mechanical protection. The inductance of each coil was measured using an M4070 LCR meter—an auto-ranging device capable of operating up to 500 kHz, well-suited for measuring low inductance and capacitance values. The meter uses an LC oscillation method to measure inductance up to 100 H. The inductances of the transmitter and receiver coils were found to be 34.3 mH and 34.5 mH, respectively, confirming their identical design. The measured values were slightly higher than theoretical estimates due to the added inductance introduced by external wiring. Mutual inductance between the coils was also determined based on their self-inductance values and equivalent series parameters using the standard formula:

$$M = \frac{L_T+L_R+L_{eq}}{2} \quad (19)$$

III. DESIGN OF SYSTEM PARAMETERS

The sample model of a wireless power structured scheme was designed by choosing the appropriate electrode size and the extreme power transfer along the load Permanent Magnet Synchronous Motor (PMSM) drive scheme. Electrode size is based on the standard of the American Wire Gauge (AWG), set at 2 mm. Self-inductance can be calculated using (13), which incorporates the input geometry of wireless coils, with

estimates for the amount of turns N, the outer diameter D_0, and the length of wire (L^{th}) obtained by working on calculating the freeware coil inductance, Coil64. The system's resonant frequency was evaluated under load conditions with a large air gap and no controllers, by observing the transmitter and recovery voltage and current waveforms. To ensure compatibility with motor control requirements, the PMSM's voltage and power capacity—ranging from 80 W at 48 V to 295 W at 50 V—were compared with the simulated system output. Mutual inductance was also estimated using equation (19). Simulations were performed under three load conditions (quarter-load, half-load, and full-load) and at varying coil distances (7.5 cm, 10 cm, and 12.5 cm), with tuning of controllers D1 and D2. The complete simulation model was constructed using the parameters listed below for the transmitter and receiver circuit: R_1= 3.3 kΩ; R_2= 2.2 kΩ; R_3= 6.8 kΩ; R_4= R_6= 15 kΩ; R_5= 10 kΩ; R_7 = R_8= 100 kΩ; R_9= 4.7 kΩ; C_1= 470 µF; C_2= 1 nF; C_3 and C_4= 2.2 nF; C_5= C_6= C_7= C_8= C_{10}=100 nF; C_9= 4.7 nF; L_1= 36 µH; L_2= 36 µH; L_3= 1 µH; C_{11}= 168 nF; R_{11}= 120 kΩ; C_{12}= 470 µF; C_{13}= 10 µF; C_{14}= 1 nF.

IV. EXPERIMENTAL AND SIMULATION RESULTS

The WPT system was evaluated under quarter-load, half-load, and full-load conditions to assess its performance across varying transmission distances and load variations between the transmitter and receiver coils (Figure 2). The motor maintained a constant rotational speed of 506.4 rpm throughout the tests.

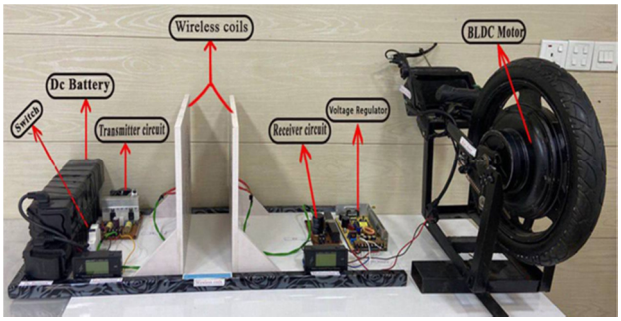

Fig. 2. Prototype for experimental tests.

Each load condition was examined at three transmission distances: 7.5 cm, 10 cm, and 12.5 cm. During each test, system parameters were measured, including input voltage and current from the battery, voltage and current at the transmitter and receiver coils, and the output power delivered to the motor. Transmission efficiency was then calculated at each stage. Simulation results, shown in Table I, aligned well with experimental data, with a maximum percentage error of 0.8% across all test conditions. All practical results for efficiency calculations are listed in Tables II and III.

It is important to note that the transmission efficiency is calculated based on DC input and power output. In Table III, it can be observed that at a specific transmission distance, the efficiency remains relatively consistent across the three load conditions. For instance, at 7.5 cm, the transmission efficiency for all three load conditions (quarter-load, half-load, and full-load) was 71.7%, 73.8%, and 72.4%, respectively. However, efficiency was significantly impacted by the transmission length at a given load current. Under quarter-load conditions, efficiency dropped from 71.7% at 7.5 cm to 50.5% at 12.5 cm.

TABLE I. COMPARISON BETWEEN SIMULATION AND EXPERIMENTAL VOLTAGE VALUES

Distance [cm]	Tx Voltage [V]		Error [%]	Rx Voltage [V]		Error [%]
	Sim.	Exp.		Sim.	Exp.	
Quarter-Load Mode						
7.5	102	101	0.8	162	162	0.06
10	114	115	0.7	251	253	0.63
12.5	126	126	0.3	297	298	0.06
Half-Load Mode						
7.5	102	101	0.8	195	195	0.4
10	145	144	0.50	244	244	0.28
12.5	204	204	0.09	244	244	0.04
Full-Load Mode						
7.5	126	126	0.30	204	204	0.39
10	199	198	0.25	243	244	0.24
12.5	254	253	0.43	279	278	0.39

TABLE II. RESULTS OF EXPERIMENTAL TESTS FOR EFFICIENCY CALCULATION (PART I)

Distance [cm]	I_{DC} Input [A]	V_{DC} Input [V]	Input Power [W]	V_{rms} Tx [V]	I_{rms} Tx [A]	I_{DC} Output [A]
Quarter-Load Mode						
7.5	1.4	105.6	147.8	101	1.955	2.2
10	1.7	104.8	178.2	115	2.45	2.4
12.5	2.1	104.2	218.8	126	2.93	2.3
Half-Load Mode						
7.5	2.2	103.4	227.5	101	1.96	3.5
10	2.5	103	257.5	144	2.93	3.48
12.5	2.9	102.3	296.7	204	3.00	3.4
Full-Load Mode						
7.5	3.4	99.8	339.3	126	1.22	5.2
10	3.7	100.9	373.3	198	2.45	5.2
12.5	4.3	99.8	429.1	253	3.00	5.13

TABLE III. RESULTS OF EXPERIMENTAL TESTS FOR EFFICIENCY CALCULATION (PART II)

Distance [cm]	V_{DC} Output [V]	Output Power [W]	I_{rms} Rx [A]	V_{rms} Rx [V]	Efficiency [%]
Quarter-Load Mode					
7.5	48.1	105.8	0.935	162	71.7
10	48.1	115.4	0.76	253	64.7
12.5	48.1	110.6	1.54	298	50.5
Half-Load Mode					
7.5	48	168	0.76	195	73.8
10	48	167.0	1.075	244	64.8
12.5	48	163.2	1.39	244	55.0
Full-Load Mode					
7.5	47.3	245.9	0.55	204	72.4
10	47.2	245.4	1.39	244	65.7
12.5	47.2	242.1	1.45	278	56.4

To convey the effectiveness of the proposed WPT system and the quality of the transmitted signal from the transmitter (Tx) to the receiver (Rx), Figures 3 and 4 present the actual voltage and current waveforms of both Tx and Rx coils at a 10 cm transmission distance under full-load conditions. The close alignment between Tx and Rx waveforms confirms the system's high transmission efficiency.

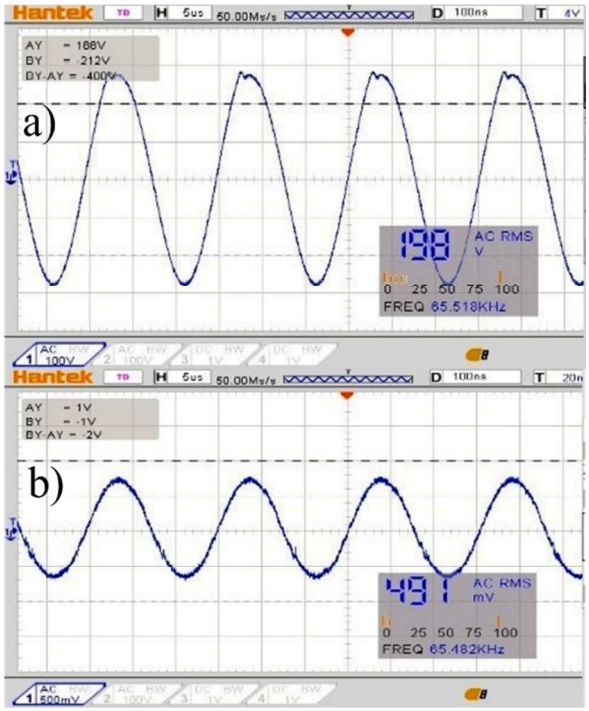

Fig. 3. Outcomes of the Tx side at full-load conditions with an airgap distance of 10 cm, a) voltage, b) current.

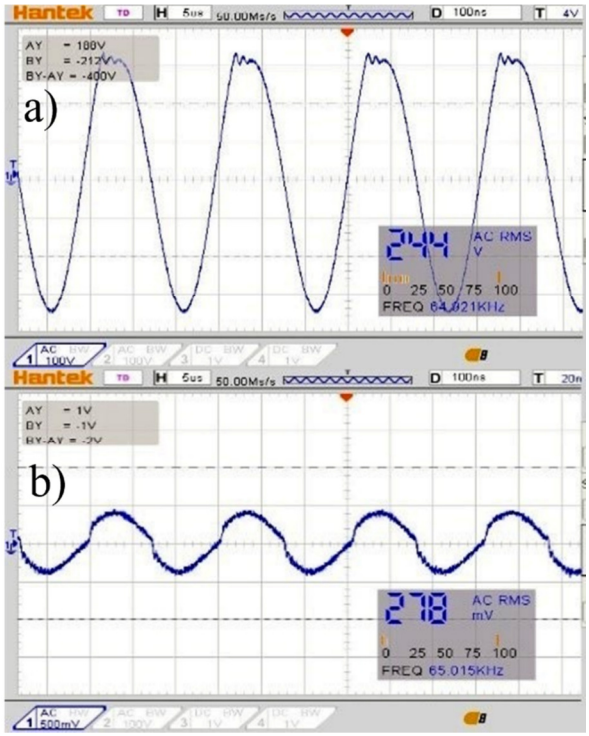

Fig. 4. Outcomes of the Rx side at full-load conditions with an airgap distance of 10 cm, a) voltage, b) current.

The boundaries of the controllers' parameters were also analyzed across three load conditions under varying distances. In the quarter-load condition, D1 and D2 were 0.02 and 0.875 at 7.5 cm, 0.13 and 0.783 at 10 cm, and 0.21 and 0.812 at 12.5 cm. Under the half-load condition, D1 and D2 values were 0.02 and 0.745 at 7.5 cm, increasing to 0.31 and 0.75 at 10 cm, and reaching 0.51 and 0.709 at 12.5 cm. In the full-load condition, D1 and D2 started at 0.21 and 0.784 at 7.5 cm, rising to 0.497 and 0.741 at 10 cm, and peaking at 0.842 and 0.715 at 12.5 cm. These results indicate that D1 and D2 parameters vary significantly with both load level and transmission distance.

V. STABILITY ANALYSIS

The stability of the WPT system is governed by control parameters on both the transmitting (Tx) and receiving (Rx) sides, as well as by the system's hardware components. While hardware parameters remain constant, the load resistance Z_L (ω_r, T) and mutual inductor M (d, K) vary depending on the system's operating conditions. The controller boundary values, specifically D1 and D2, are closely linked to Z_L and M.

The study identifies a motor speed range conducive to stable operation, estimated to be between 68.97 rad/s and 86.20 rad/s. The data further illustrate the relationship between load impedance and system stability under two distinct configurations—D1 and D2. In the D1 configuration, the system maintains stable operation across load impedances ranging from 115 Ω to 40 Ω, with corresponding stability factors decreasing from 0.350 to 0.150. In contrast, the D2 configuration remains stable within a narrower impedance range of 25 Ω to 20 Ω, with stability factors slightly increasing from 0.760 to 0.800.

VI. COMPARATIVE STUDY

A comparison of WPT systems from various studies reveals notable differences in operating frequency, power level, transmission distance, and efficiency. For example, systems like KAIST [23] operate at a low frequency of 20 kHz and transmit 60 kW over 20 cm, achieving a relatively lower efficiency of 85%. In contrast, studies [24, 25] report the highest efficiency—97.52%—at 86.5 kHz for a 7.7 kW transfer over 10 cm. Meanwhile, the proposed WPT system operates at 65 kHz, delivering 0.25 kW over 7.5 cm with a notable efficiency of 94.75%, demonstrating a well-optimized balance between frequency, power, distance, and efficiency [26]. Other systems designed for higher power and extended transmission distances, such as those in [27, 28], maintain efficiency levels between 90% and 95%. The proposed system aligns well with these studies, offering competitive efficiency while targeting specific design parameters [29].

VII. CONCLUSIONS

The study developed an inductive Wireless Power Transfer (WPT) system tailored for In-Wheel Motor (IWM) applications. This system underwent design and testing under various load conditions and different distances between the transmitting (Tx) and receiving (Rx) coils. During these tests, critical parameters were meticulously measured, such as contribution voltage and current from the battery, the voltage and the current in both (Tx and Rx) coils, and power output to the Permanent Magnet Synchronous Motor (PMSM). The system's efficiency was evaluated based on the DC input and output power for each test case. Experimental results

demonstrated that WPT efficiency is strongly influenced by the distance between the Tx and Rx coils, primarily due to the reduction in coupling coefficient as the gap increases. For instance, efficiency dropped from 71.7% to 50.5% once the air gap distance expanded from 7.5 cm to 12.5 cm in quarter-load conditions. In contrast, the effect of loading on efficiency at a fixed distance was minimal. Furthermore, simulation results validated the system's capability to wirelessly power the IWM.

REFERENCES

[1] A. Triviño, J. M. González-González, and J. A. Aguado, "Wireless Power Transfer Technologies Applied to Electric Vehicles: A Review," *Energies*, vol. 14, no. 6, Mar. 2021, Art. no. 1547, https://doi.org/10.3390/en14061547.

[2] I. Okasili, A. Elkhateb, and T. Littler, "A Review of Wireless Power Transfer Systems for Electric Vehicle Battery Charging with a Focus on Inductive Coupling," *Electronics*, vol. 11, no. 9, Apr. 2022, Art. no. 1355, https://doi.org/10.3390/electronics11091355.

[3] B. Kallel, O. Kanoun, and H. Trabelsi, "Large air gap misalignment tolerable multi-coil inductive power transfer for wireless sensors," *IET Power Electronics*, vol. 9, no. 8, pp. 1768–1774, Jun. 2016, https://doi.org/10.1049/iet-pel.2015.0800.

[4] A. J. Mahdi, S. Fahad, and W. Tang, "An Adaptive Current Limiting Controller for a Wireless Power Transmission System Energized by a PV Generator," *Electronics*, vol. 9, no. 10, Oct. 2020, Art. no. 1648, https://doi.org/10.3390/electronics9101648.

[5] X. Cheng, T. Chen, J. Li, and J. Wang, "Coordinated Control Method for Lateral Stability and Differential Power-Assisted Steering of In-Wheel Motor Drive Electric Vehicles," *World Electric Vehicle Journal*, vol. 14, no. 8, Jul. 2023, Art. no. 200, https://doi.org/10.3390/wevj14080200.

[6] M. T. Nguyen *et al.*, "Electromagnetic Field Based WPT Technologies for UAVs: A Comprehensive Survey," *Electronics*, vol. 9, no. 3, Mar. 2020, Art. no. 461, https://doi.org/10.3390/electronics9030461.

[7] A. P. Sample, B. H. Waters, S. T. Wisdom, and J. R. Smith, "Enabling Seamless Wireless Power Delivery in Dynamic Environments," *Proceedings of the IEEE*, vol. 101, no. 6, pp. 1343–1358, Jun. 2013, https://doi.org/10.1109/JPROC.2013.2252453.

[8] Y. Li, J. Liu, Q. Yang, X. Ni, Y. Zhai, and Z. Lou, "Directional Characteristics of Wireless Power Transfer via Coupled Magnetic Resonance," *Electronics*, vol. 9, no. 11, Nov. 2020, Art. no. 1910, https://doi.org/10.3390/electronics9111910.

[9] S. Li and C. C. Mi, "Wireless Power Transfer for Electric Vehicle Applications," *IEEE Journal of Emerging and Selected Topics in Power Electronics*, vol. 3, no. 1, pp. 4–17, Mar. 2015, https://doi.org/10.1109/JESTPE.2014.2319453.

[10] A. Zakerian, S. Vaez-Zadeh, and A. Babaki, "A Dynamic WPT System With High Efficiency and High Power Factor for Electric Vehicles," *IEEE Transactions on Power Electronics*, vol. 35, no. 7, pp. 6732–6740, Jul. 2020, https://doi.org/10.1109/TPEL.2019.2957294.

[11] K. Cakir and A. Sabanovic, "In-wheel motor design for electric vehicles," in *9th IEEE International Workshop on Advanced Motion Control, 2006.*, Istanbul, Turkey, 2006, pp. 613–618, https://doi.org/10.1109/AMC.2006.1631730.

[12] A. J. Mahdi, H. A. Saber, A. M. Ridha, and M. J. Mohammed, "Comparative analysis of different inverters and controllers to investigate performance of electrosurgical generators under variable tissue impedance," *Acta Innovations*, no. 48, pp. 61–74, May 2023, https://doi.org/10.32933/ActaInnovations.48.5.

[13] S. Sakai, H. Sado, and Y. Hori, "Motion control in an electric vehicle with four independently driven in-wheel motors," *IEEE/ASME Transactions on Mechatronics*, vol. 4, no. 1, pp. 9–16, Mar. 1999, https://doi.org/10.1109/3516.752079.

[14] S. Murata, "Innovation by in-wheel-motor drive unit," *Vehicle System Dynamics*, vol. 50, no. 6, pp. 807–830, Jun. 2012, https://doi.org/10.1080/00423114.2012.666354.

[15] K. Deepak, M. A. Frikha, Y. Benômar, M. El Baghdadi, and O. Hegazy, "In-Wheel Motor Drive Systems for Electric Vehicles: State of the Art, Challenges, and Future Trends," *Energies*, vol. 16, no. 7, Mar. 2023, Art. no. 3121, https://doi.org/10.3390/en16073121.

[16] K. M. Rahman, N. R. Patel, T. G. Ward, J. M. Nagashima, F. Caricchi, and F. Crescimbini, "Application of Direct-Drive Wheel Motor for Fuel Cell Electric and Hybrid Electric Vehicle Propulsion System," *IEEE Transactions on Industry Applications*, vol. 42, no. 5, pp. 1185–1192, Sep. 2006, https://doi.org/10.1109/TIA.2006.880886.

[17] M. Sato, G. Yamamoto, D. Gunji, T. Imura, and H. Fujimoto, "Development of Wireless In-Wheel Motor Using Magnetic Resonance Coupling," *IEEE Transactions on Power Electronics*, vol. 31, no. 7, pp. 5270–5278, Jul. 2016, https://doi.org/10.1109/TPEL.2015.2481182.

[18] H. Fujimoto, O. Shimizu, S. Nagai, T. Fujita, D. Gunji, and Y. Ohmori, "Development of Wireless In-wheel Motors for Dynamic Charging: From 2nd to 3rd generation," in *2020 IEEE PELS Workshop on Emerging Technologies: Wireless Power Transfer (WoW)*, Seoul, Korea (South), Nov. 2020, pp. 56–61, https://doi.org/10.1109/WoW47795.2020.9291287.

[19] T. Takeuchi, T. Imura, H. Fujimoto, and Y. Hori, "Power management of Wireless In-Wheel Motor by SOC control of wheel side Lithium-ion Capacitor," in *IECON 2016 - 42nd Annual Conference of the IEEE Industrial Electronics Society*, Florence, Italy, Oct. 2016, pp. 4547–4552, https://doi.org/10.1109/IECON.2016.7793109.

[20] F. Jolani, Y. Yu, and Z. Chen, "A Planar Magnetically Coupled Resonant Wireless Power Transfer System Using Printed Spiral Coils," *IEEE Antennas and Wireless Propagation Letters*, vol. 13, pp. 1648–1651, 2014, https://doi.org/10.1109/LAWP.2014.2349481.

[21] *Coil64*, (v.2.2.34), Coil32 - the coil inductance calculator. [Online]. Available: https://coil32.net/download-coil64-for-windows.html.

[22] *Flat Spiral Coil Calculator*, (2004), Promina Electronics Design. [Online]. Available: http://www.pronine.ca/spiralcoil.htm.

[23] A. Visvizi and O. Troisi, *Managing Smart Cities: Sustainability and Resilience Through Effective Management*, 1st ed., Springer, 2022.

[24] F. Grazian, T. B. Soeiro, and P. Bauer, "Voltage/Current Doubler Converter for an Efficient Wireless Charging of Electric Vehicles With 400-V and 800-V Battery Voltages," *IEEE Transactions on Industrial Electronics*, vol. 70, no. 8, pp. 7891–7903, Aug. 2023, https://doi.org/10.1109/TIE.2022.3208582.

[25] Z. Kadhim, L. Hammed, F. Rahima, and A. Ridha, "Elastohydrodynamic analysis of a journal bearing with different grade oils considering thermal and cavitation effects using CFD-FSI," *Diagnostyka*, vol. 24, no. 2, pp. 1–10, May 2023, https://doi.org/10.29354/diag/166102.

[26] G. Shahgholian and A. Fattollahi, "Improving Power System Stability Using Transfer Function: A Comparative Analysis," *Engineering, Technology & Applied Science Research*, vol. 7, no. 5, pp. 1946–1952, Oct. 2017, https://doi.org/10.48084/etasr.1341.

[27] S. Laporte, G. Coquery, V. Deniau, A. De Bernardinis, and N. Hautière, "Dynamic Wireless Power Transfer Charging Infrastructure for Future EVs: From Experimental Track to Real Circulated Roads Demonstrations," *World Electric Vehicle Journal*, vol. 10, no. 4, Nov. 2019, Art. no. 84, https://doi.org/10.3390/wevj10040084.

[28] Z. Wang, X. Wei, and H. Dai, "Design and Control of a 3 kW Wireless Power Transfer System for Electric Vehicles," *Energies*, vol. 9, no. 1, Dec. 2015, Art. no. 10, https://doi.org/10.3390/en9010010.

[29] M. E. Bendib and A. Mekias, "Solar Panel and Wireless Power Transmission System as a Smart Grid for Electric Vehicles," *Engineering, Technology & Applied Science Research*, vol. 10, no. 3, pp. 5683–5688, Jun. 2020, https://doi.org/10.48084/etasr.3473.